BBA - Molecular and Cell Biology of Lipids 1869 (2024) 159510

Contents lists available at ScienceDirect

BBA - Molecular and Cell Biology of Lipids

journal homepage: www.elsevier.com/locate/bbalip

Elucidation of molecular mechanisms by which amyloid β_{1-42} fibrils exert cell toxicity

Kiryl Zhaliazka [a], Dmitry Kurouski [a,b,*]

[a] Department of Biochemistry and Biophysics, Texas A&M University, College Station, TX 77843, United States
[b] Department of Biomedical Engineering, Texas A&M University, College Station, TX 77843, United States

ARTICLE INFO

Keywords:
Amyloid β_{1-42}
Endoplasmic reticulum
Unfolded protein response
Mitochondria
Lipids

ABSTRACT

Abrupt aggregation of amyloid β_{1-42} ($A\beta_{1-42}$) peptide in the frontal lobe is the expected underlying cause of Alzheimer's disease (AD). β-Sheet-rich oligomers and fibrils formed by $A\beta_{1-42}$ exert high cell toxicity. A growing body of evidence indicates that lipids can uniquely alter the secondary structure and toxicity of $A\beta_{1-42}$ aggregates. At the same time, underlying molecular mechanisms that determine this difference in toxicity of amyloid aggregates remain unclear. Using a set of molecular and biophysical assays to determine the molecular mechanism by which $A\beta_{1-42}$ aggregates formed in the presence of cholesterol, cardiolipin, and phosphatidylcholine exert cell toxicity. Our findings demonstrate that rat neuronal cells exposed to $A\beta_{1-42}$ fibrils formed in the presence of lipids with different chemical structure exert drastically different magnitude and dynamic of unfolded protein response (UPR) in the endoplasmic reticulum (ER) and mitochondria (MT). We found that the opposite dynamics of UPR in MT and ER in the cells exposed to $A\beta_{1-42}$: cardiolipin fibrils and $A\beta_{1-42}$ aggregates formed in a lipid-free environment. We also found that $A\beta_{1-42}$: phosphatidylcholine fibrils upregulated ER UPR simultaneously downregulating the UPR response of MT, whereas $A\beta_{1-42}$: cholesterol fibrils suppressed the UPR response of ER and upregulated UPR response of MT. We also observed progressively increasing ROS production that damages mitochondrial membranes and other cell organelles, ultimately leading to cell death.

1. Introduction

Alzheimer's disease (AD) is a severe pathology caused by the progressive degeneration of neurons in the frontal lobe and other brain regions. [1–6] As a result, drastic impairment of cognitive abilities and short-term memory are developed by AD patients. Some pieces of experimental evidence indicate that the progressive neuronal death can be caused by amyloid oligomers and fibrils. [7–14] These highly toxic aggregates are formed by both amyloid β_{1-40} ($A\beta_{1-40}$) and amyloid β_{1-42} ($A\beta_{1-42}$) peptides. [15,16] These aggregates can also propagate from cell to cell via *endo-* and exocytosis, which causes the spread of AD ultimately resulting in brain atrophy. [1–7,17]

Numerous pieces of experimental evidence demonstrate that the rate of $A\beta_{1-40}$ and $A\beta_{1-42}$ aggregation can be uniquely altered by several biological molecules, such as fatty acids, neurotransmitters, and lipids. [18–22] For instance, Eto and co-workers demonstrated that docosahexaenoic acid (DHA), an omega-3 fatty acid, drastically accelerated the aggregation rate of $A\beta_{1-40}$. [19] Furthermore, morphologically different fibrils were formed by $A\beta_{1-40}$ in the presence of DHA. These fibrils had significantly different cell toxicity. Khatua and co-workers found that lauric acid could stabilize $A\beta_{1-42}$ oligomers. [20] Similar findings were reported by Johansson and co-workers for DHA. [22] It was also found that the toxicity of $A\beta_{1-42}$ fibrils could be uniquely altered by the DHA concentration present at the protein aggregation stage. Cataldi and et al. found that 3,4-dihydroxyphenylacetaldehyde, a molecule formed as a result of dopamine oxidation, could change the secondary structure of $A\beta_{1-40}$ oligomers. [21] The researchers found that such oligomers exerted significantly higher cytotoxicity compared to $A\beta_{1-40}$ fibrils. Recently reported results by our group showed that cardiolipin (CL), phosphatidylcholine (PC), and cholesterol (Cho) drastically increased the rate of $A\beta_{1-42}$ aggregation and altered the secondary structure of both oligomers and fibrils if present at 1:1 M ratio with the peptide. [23] Some experimental studies showed that fibrils exhibited greater toxicity among all the aggregates than oligomers or protofibrils. [23]

Abbreviations: MT, mitochondria; UPR, unfolded protein response; AD, Alzheimer's disease; ER, endoplasmic reticulum; CL, cardiolipin; LUVs, large unilamellar vesicles; PC, phosphatidylcholine; LDH, lactate dehydrogenase.

* Corresponding author at: Department of Biochemistry and Biophysics, Texas A&M University, College Station, TX 77843, United States.
E-mail address: dkurouski@tamu.edu (D. Kurouski).

https://doi.org/10.1016/j.bbalip.2024.159510
Received 28 March 2024; Received in revised form 6 May 2024; Accepted 8 May 2024
Available online 15 May 2024

Additionally, our findings revealed that $A\beta_{1-42}$ oligomers and fibrils formed under these experimental conditions retained lipids in their structure. As a result, $A\beta_{1-42}$ oligomers formed in the presence of lipids exerted significantly higher cell toxicity compared to $A\beta_{1-42}$ oligomers grown in the lipid-free environment. Matveyenka et al. showed that insulin and lysozyme stability could be altered by lipids. [24–29] However, it was found that phospho- and sphingolipids decreased the toxicity of lysozyme and insulin fibrils. Similar findings were previously made for other amyloidogenic proteins, such as α-synuclein (α-syn) and amylin. [2,30–35] Recently reported results by Sitton and co-workers demonstrated that choline plasmalogens (CPs), a uniquely class of phospholipids, drastically lowered the toxicity of transthyretin fibrils

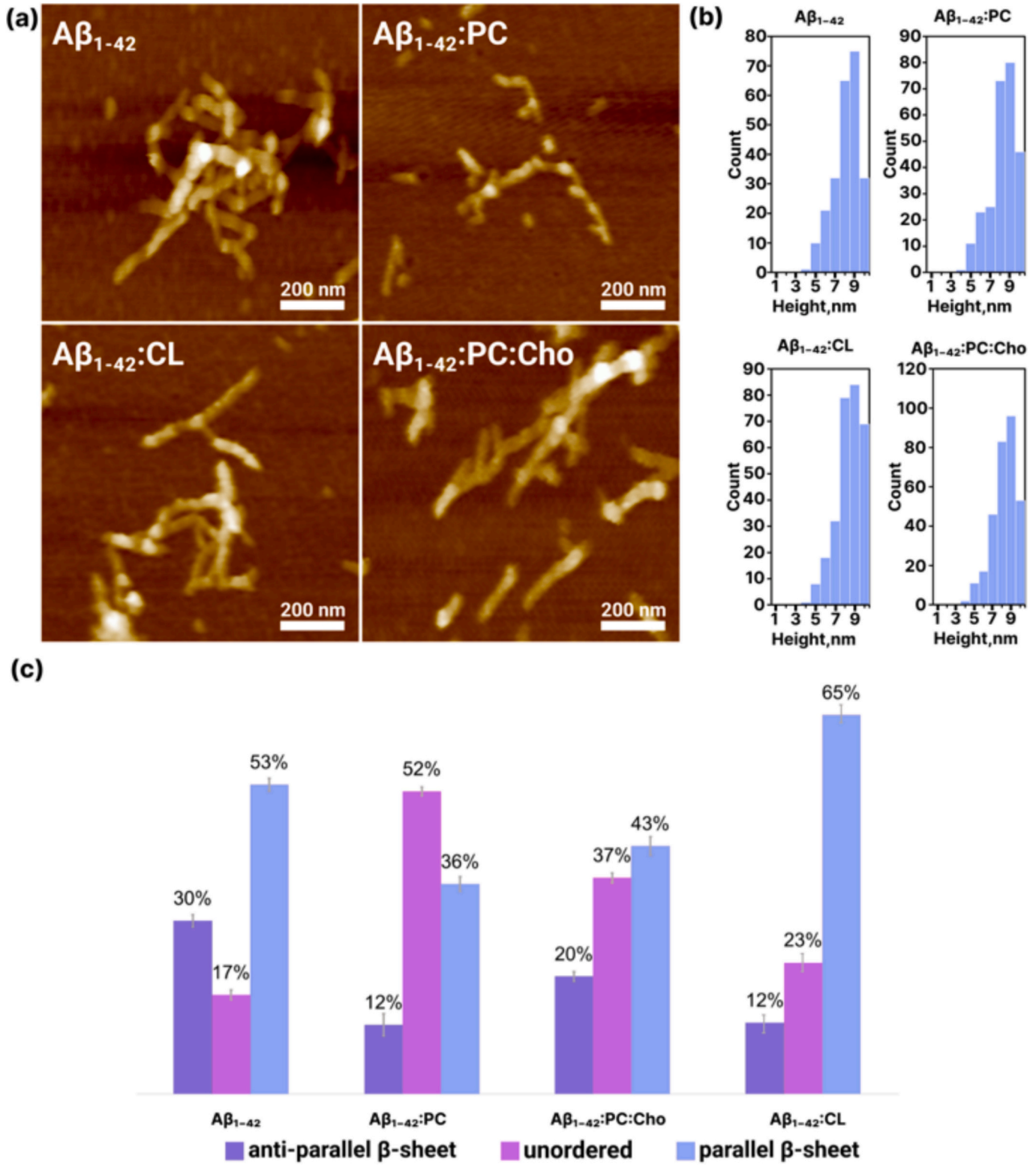

Fig. 1. AFM height images (a) and height profile (b) of Aβ fibrils formed after 72 h of protein aggregation with and without PC, CL, and PC:Cho LUVs. Histograms (c) of the amounts of unordered protein, parallel and anti-parallel β-sheet in the analyzed protein aggregates.

that were formed in their presence [36]. However, this effect of CPs was not evident for α-syn fibrils [37].

The question to ask is how lipids change the toxicity of amyloid aggregates. Experimental results reported by Matveyenka and co-workers showed that insulin fibrils formed in the presence of different lipids could be endocytosed by cells. [28] This resulted in severe damage to late endosomes and the escape of toxic protein aggregates to the cell cytosol. It was also shown that α-syn fibrils formed in the presence of lipids with different structures exerted dissimilar magnitudes of endosomal damage. [38] Thus, one can expect that the chemical nature of lipids present in such aggregates determines their cytotoxicity. These results are in a good agreement with the proposed by La Rosa group lipid-chaperone hypothesis. [39–41] It was shown that membrane lipids could interact with amyloidogenic proteins forming stable lipid-in-protein complexes. [39–41] La Rosa group also showed that membranes dominated with lipids that have high critical micelle concentration (cmc) suppressed fibril formation. However, lipids with low cmc, on the opposite, facilitated fibril formation [42,43] Thus, the chemical nature of the lipid molecules correlates with the toxicity exerted by lipid: protein aggregates.

In this study, we employed real-time polymerase chain reaction (rt-PCR) to investigate the extent to which changes in the expression rates of proteins involved in unfolded protein response (UPR) depend on the chemical structure of protein-lipid aggregates. After we exposed N27 cells to $A\beta_{1-42}$ fibrils formed in the presence of CL, PC, and Cho, rt-PCR of genes responsible for MT and ER responses to unfolded proteins was performed. Our results show that cells upregulate genes responsible for ER UPR simultaneously downregulating genes that control MT stress. These results suggest that cells maximize MT activity aiming to mitigate ER stress and restore normal cell functioning. However, if cells were failing to suppress the UPR-driven ER stress, apoptotic mechanisms were engaged.

2. Results

2.1. Structural and morphological characterization of $A\beta_{1-42}$ fibrils

After 72 h of protein aggregation under the lipid-free environment, $A\beta_{1-42}$ formed long fibril-like species that had 8–10 nm in height, Fig. 1 (a, b).

Morphologically similar fibrils were found in $A\beta_{1-42}$:PC, $A\beta_{1-42}$:CL, and $A\beta_{1-42}$:PC:Cho. These aggregates had the same heights as $A\beta_{1-42}$ fibrils formed under the lipid-free environment. Previously reported by our group nano-Infrared analysis of these fibrils revealed drastic differences in their secondary structure. [23] We found that the secondary structure of $A\beta_{1-42}$ fibrils was dominated by parallel β-sheet (55 %) with 21 % and 24 % of anti-parallel β-sheet and unordered protein secondary structure, respectively, Fig. 1 (c). $A\beta_{1-42}$:PC fibrils had significantly greater amount of disordered protein in the secondary structure, whereas the secondary structure of $A\beta_{1-42}$:PC:Cho fibrils had nearly equal propensity presence of parallel-, anti-parallel β-sheet and disordered protein secondary structure. Finally, $A\beta_{1-42}$:CL had the highest percentage of parallel β-sheet relative to all other aggregates with the lowest percentage of disordered protein in the secondary structure.

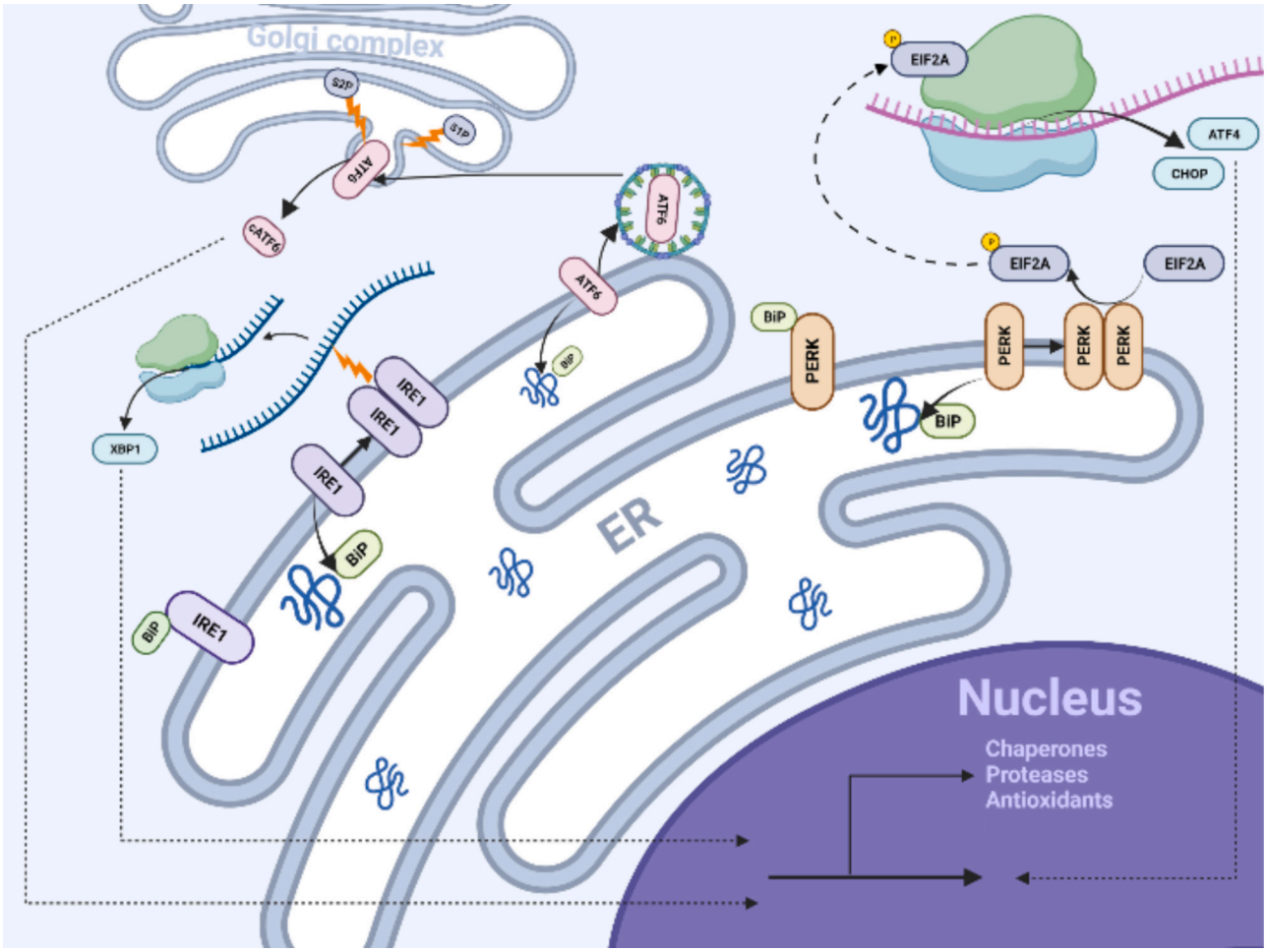

Scheme 1. Schematic illustration of UPR pathways in ER triggered by unfolded protein.

2.2. Elucidation of UPR-mediated ER stress exerted by $A\beta_{1-42}$ fibrils

The UPR activates three transmembrane proteins localized in ER: PKR-like ER kinase (PERK), Inositol Requiring 1 (IRE1), and Activating Transcription Factor 6 (ATF6), Scheme 1. [44–46] The activation of these proteins is regulated by glucose-regulated chaperon with molecular weight of 78 kDa named GRP78 or BiP. [47,48]

The phosphorylation of PERK, which is a type I ER transmembrane kinase, activates eukaryotic initiation factor 2 (eIF2a). [49–52] Phosphorylated eIF2a inhibits the compilation of ribosomal complexes that initiate the translation of mRNA. [52] As a result, protein expression, and consequently, the ER workload are suppressed by cells. eIF2a also facilitates the expression of an activating transcription factor ATF4 involved in cell apoptosis. ATF4 activates C-EBP Homologous Protein (CHOP), factor that regulates the expression of caspase 3 kinase, as well as BCL2 protein family members. [53,54]

We found that the relative expression of PERK did not change after 6 h of cell exposure to $A\beta_{1-42}$ fibrils formed in the lipid-free environment. However, we observed a gradual increase in PERK expression to 1.27-fold at 12 h and 1.81-fold at 24 h. The relative expression of eif2a increased by 1.08-fold at 6 h, followed by a slight increase to 1.30-fold at 12 h and a decrease to 0.84-fold at 24 h. We also found that the relative expression of ATF4 increased by 1.62-fold at 6 h, followed by a slight increase to 1.73-fold at 12 h and a significant increase to 2.70-fold at 24 h. The relative expression of CHOP increased by 1.62-fold at 6 h, as a response to $A\beta_{1-42}$ fibrils formed in the lipid-free environment, followed by a decrease to 0.83-fold at 12 h and an increase to 1.56-fold at 24 h (Fig. 2).

Our results also showed that $A\beta_{1-42}$:PC fibrils caused drastically different changes in the expression levels of PERK, eif2a, ATF4, and CHOP compared to the expression levels of these factors observed upon the exposition of N27 cells to $A\beta_{1-42}$ fibrils formed in the lipid-free environment. Specifically, we found an increase in the expression of PERK of 4.45-fold at 6 h with a subsequent increase to 5.03 and 6.67 at 12, and 24 h, respectively. The relative expression levels of eif2a decreased with time (0.74, 0.61, and 0.58 at 6, 12, and 24 h, respectively). We also found that relative expression levels of ATF4 increased with time (5.98, 5.43, and 7.61 at 6, 12, and 24 h, respectively). Interestingly, the relative expression levels of CHOP significantly decreased at 6 and 12 h (0.15 and 0.14, respectively), but increased at 24 h (1.84).

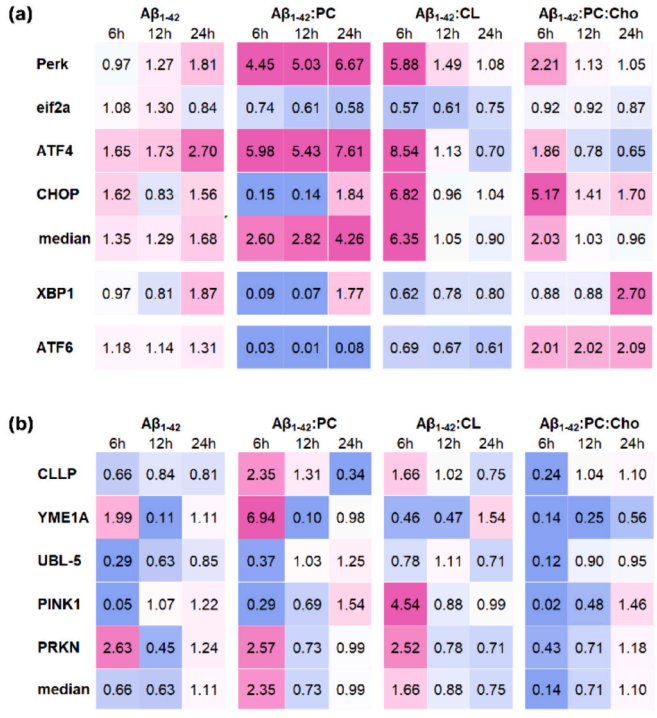

Fig. 2. (a) Heat map of up (red) and downregulated (blue) ER (a) and MT UPR (b) genes expression after N27 cells were exposed to $A\beta_{1-42}$, $A\beta_{1-42}$:PC, $A\beta_{1-42}$:CL, and $A\beta_{1-42}$:PC:Cho fibrils for 6 h, 12 h, and 24 h. (For interpretation of the references to colour in this figure legend, the reader is referred to the web version of this article.)

$A\beta_{1-42}$:CL fibrils enabled drastically different changes in the expression levels of PERK, eif2a, ATF4, and CHOP compared to the expression levels of these factors observed upon the exposition of N27 cells to both $A\beta_{1-42}$ and $A\beta_{1-42}$:PC fibrils. Specifically, we found that the expression of PERK was significantly upregulated at 6 h (5.48-fold) but downregulated at 12 h (1.49-fold) and 24 h (1.08-fold). The relative expression of eif2a was downregulated at 6 h (0.57-fold), at 12 h (0.61-fold), and at 24 h (0.75-fold). The expression of ATF4 was significantly upregulated at 6 h (8.54-fold) then decreased at 12 h (1.13-fold) and downregulated at 24 h (0.70-fold). CHOP expression was upregulated at 6 h (6.82-fold) and 24 h (1.04-fold) but downregulated at 12 h (0.96-fold).

Finally, for the N27 cells exposed to $A\beta_{1-42}$:PC:Cho, we observed a decrease in PERK expression at 12 h (1.13-fold) and 24 h (1.05-fold) compared to the 6 h time point (2.21-fold). Similarly, the expression of eif2a decreased slightly from 6 h (0.92-fold) to 24 h (0.87-fold) time points. Interestingly, the expression ATF4 showed a gradual decrease from 6 h (1.86-fold) to 24 h (0.65-fold). In contrast, the expression of CHOP decreased at 12 h (1.41-fold) and 24 h (1.70-fold) compared to 6 h (5.17-fold). These results indicated that although all analyzed protein aggregates activated the PERK pathway of UPR, the dynamics of these responses were unique for each of the aggregates. We also found that different protein aggregates exhibited different magnitudes of the expression of PERK kinase. Based on these results, we can make a conclusion that the secondary structure of Aβ fibrils, as well as the lipids present in their structure, uniquely alters the UPR response of N27 cells to these aggregates.

IRE1 is a type I ER kinase localized in the cell membrane. IRE1 is activated by unfolded or misfolded proteins. [52] This results in IRE1 dimerization. IRE1 dimers then auto-phosphorylate splicing of mRNA X Box Binding factor 1 (XBP-1) [49–51]. Spliced mRNA encodes a basic zipper leucine transcription factor (b-ZIP), which in turn causes upregulation of UPR genes. b-ZIP also upregulates genes which encode protein disulfide isomerase and chaperones that help to facilitate protein folding. [49–51].

Our results show that the relative expression of XBP-1 decreased slightly by 0.97-fold at 6 h, followed by a further decrease to 0.81-fold at 12 h and an increase to 1.87-fold at 24 h as a response to $A\beta_{1-42}$ fibrils formed in the lipid-free environment. We also that $A\beta_{1-42}$:PC fibrils caused a slight downregulation of XBP-1 to 0.09- and 0.07-fold at 6 h and 12 h, respectively. However, a strong increase in the expression of this factor was observed at 24 h for $A\beta_{1-42}$:PC fibrils (1.77-fold). Similar changes in the expression levels of XBP-1 were observed because of the exposition of N27 cells to $A\beta_{1-42}$:CL fibrils. We found that the expression of XBP1 was downregulated at 6 h (0.62-fold) as well as at 12 h (0.78-fold) and 24 h (0.80-fold). Finally, $A\beta_{1-42}$:PC:Cho increased the expression of XBP-1 at 24 h time point (2.70-fold) compared to the 6 h (0.88-fold) and 12 h (0.88-fold) time points. These results demonstrated that Aβ fibrils with drastically different secondary structure demonstrated unique dynamics of XBP-1 expression. Consequently, these aggregates uniquely alter the UPR response of neuronal cells.

ATF6 is also activated upon the ER stress. Activated ATF6 propagates to Golgi where it gets cleaved by proteases S1P and S2P that produce an active transcription factor fragment (cATF6), which is engaged in the mitigation of the ER stress. [47,48] We found that the expression of the ATF6 was moderately upregulated in response to $A\beta_{1-42}$ fibrils formed in the lipid-free environment. The relative expression of ATF6 increased by 1.18-fold at 6 h, followed by a slight decrease to 1.14-fold at 12 h and a slight increase to 1.31-fold at 24 h. Our results also showed that $A\beta_{1-42}$:

PC fibrils caused a severe downregulation of the expression of ATF6 (0.03, 0.01, and 0.08 at 6 h, 12 h, and 24 h). Similar changes in the expression levels of XBP-1 were observed because of the exposition of N27 cells to $A\beta_{1-42}$:CL fibrils. We found that the relative expression of ATF6 was downregulated at 6 h (0.69-fold) and 12 h (0.67-fold) same as at 24 h (0.61-fold). We found that $A\beta_{1-42}$:PC:Cho fibrils strongly increased the expression of ATF6 at all time points (6 6–12 h). Based on these results, we can conclude that Aβ aggregates with different secondary structures made distinctly different changes in the expression of ATF6-induced UPR.

2.3. Elucidation of UPR-mediated MT stress exerted by $A\beta_{1-42}$ fibrils

In MT, the unfolded protein response (mt-UPR) is a vital cellular mechanism that ensures proper protein folding and quality control. Several key proteins, including CLPP, YME1A, UBL-5, PINK1, and PRKN, play crucial roles in arranging the UPR response (Scheme 2).

CLPP is a protease enzyme found in the MT matrix. It assists in degrading misfolded or damaged proteins, preventing their accumulation and potential toxicity. By selectively cleaving these aberrant proteins, CLPP helps maintain MT protein homeostasis. [55]

We observed that $A\beta_{1-42}$ fibrils formed in a non-lipid environment exhibited relatively low expression levels of CLPP, with values of 0.66, 0.84, and 0.81 at 6, 12, and 24 h, respectively. In contrast, when $A\beta_{1-42}$ fibrils were formed in the presence of PC LUVs, we observed a notable increase in CLPP expression at 6 h, with a 2.35-fold change. However, CLPP expression decreased at 12 h (1.31-fold) and significantly dropped at 24 h (0.34-fold). Further analysis was conducted for $A\beta_{1-42}$ fibrils formed with CL LUVs. In this case, CLPP expression showed a relative expression of 1.66 at 6 h, followed by 1.02 at 12 h, and 0.75 at 24 h. Additionally, we explored the gene expression in samples treated with $A\beta_{1-42}$ formed in the presence of PC:Cho LUVs. The relative expression of CLPP exhibited a significant decrease at 6 h (0.24-fold), followed by a recovery to 1.04-fold at 12 h, and a slight increase to 1.10-fold at 24 h.

YME1A, another MT protease, serves as a critical component of the UPR response. It targets and degrades unfolded or misfolded proteins in the inner MT membrane space. YME1A plays a vital role in MT protein quality control by recognizing and eliminating damaged proteins, thereby preserving MT function. [56]

Notably, $A\beta_{1-42}$ fibrils formed in a non-lipid environment exhibited relatively low expression levels of YME1A, with values of 1.99 at 6 h. However, YME1A expression decreased significantly to 0.11 at 12 h before rebounding to 1.11 at 24 h. In contrast, when $A\beta_{1-42}$ fibrils were formed in the presence of PC LUVs, we observed a substantial increase in YME1A expression at 6 h, with a remarkable 6.94-fold change. However, YME1A expression decreased sharply at 12 h (0.10-fold) and only slightly increased at 24 h (0.98-fold). Furthermore, we investigated the impact of $A\beta_{1-42}$ fibrils formed with CL LUVs on YME1A expression. In this case, YME1A exhibited a relative expression of 0.46 at 6 h, followed by 0.47 at 12 h, and a notable increase to 1.54 at 24 h. Additionally, our analysis extended to the gene expression in samples treated with $A\beta_{1-42}$ formed in the presence of PC:Cho LUVs. Interestingly, the relative expression of YME1A was significantly decreased at 6 h (0.14-fold), followed by a modest recovery to 0.25-fold at 12 h, and a further increase to 0.56-fold at 24 h.

UBL-5, or Ubiquitin-like protein 5, participates in the UPR response by facilitating the clearance of damaged or unfolded proteins. UBL-5, a nuclear protein, acts as a transcriptional regulator by interacting with transcription factors such as DVE-1 and ATFS-1, modulating the expression of genes involved in mitochondrial protein folding, degradation, and dynamics, thereby playing a critical role in regulating the mt-UPR pathway and ensuring mitochondrial protein homeostasis. [57]

Ab_{1-42} fibrils formed in a non-lipid environment exhibited relatively low expression levels of UBL-5, with values of 0.29 at 6 h. However, UBL-5 expression increased to 0.63 at 12 h and further to 0.85 at 24 h. In contrast, when $A\beta_{1-42}$ fibrils were formed in the presence of PC LUVs, we observed a significant decrease in UBL-5 expression at 6 h (0.37-fold). However, UBL-5 expression rebounded and increased at 12 h (1.03-fold) and further at 24 h (1.25-fold). Furthermore, our analysis extended to Aβ1–42 fibrils formed with PC:CL LUVs. In this case, UBL-5 displayed a relative expression of 0.78 at 6 h, followed by an increase to 1.11 at 12 h, and a decrease to 0.71 at 24 h. Also, we investigated the gene expression in samples treated with $A\beta_{1-42}$ formed in the presence of PC:Cho LUVs. The relative expression of UBL-5 significantly decreased at 6 h (0.12-fold), followed by a recovery to 0.90-fold at 12 h, and a slight increase to 0.95-fold at 24 h.

PINK1 (PTEN-induced kinase 1) and PRKN (Parkin) are two proteins that work in tandem to promote MT health and integrity during the UPR response. [58] PINK1 acts as a sensor for MT dysfunction, accumulating on the outer MT membrane in response to damaged or depolarized MT. It phosphorylates both itself and PRKN, triggering the recruitment and activation of PRKN. Once activated, PRKN plays a crucial role in eliminating damaged MT through mitophagy. It ubiquitinates proteins on the surface of dysfunctional MT, signaling them for degradation and subsequent recycling. Selectively removing impaired MT, PINK1, and PRKN help maintain MT quality control and prevent the propagation of

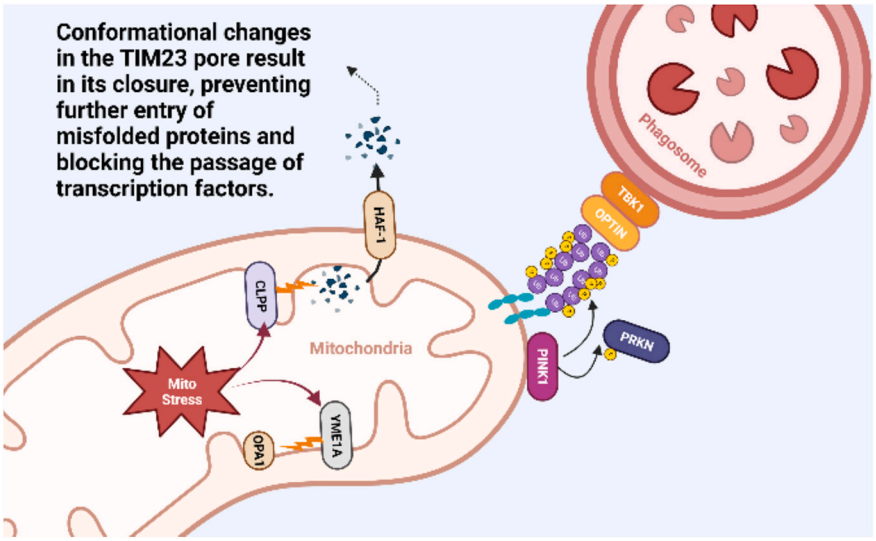

Scheme 2. Schematic illustration of MT UPR that can be activated by misfolded proteins and amyloid aggregates.

damaged organelles.

In a non-lipid environment, we observed a very low relative expression of PINK1 at 6 h (0.05-fold), which then increased to 1.07-fold at 12 h and further to 1.22-fold at 24 h. Conversely, the relative expression of PRKN was significantly higher at 6 h (2.63-fold), followed by a decrease to 0.43-fold at 12 h, and a subsequent increase to 1.24-fold at 24 h. When $A\beta_{1-42}$ fibrils were formed in the presence of PC LUVs we observed notable changes in the expression of PINK1 and PRKN. PINK1 expression decreased at 6 h (0.29-fold), increased at 12 h (0.69-fold), and significantly increased at 24 h (1.54-fold). Meanwhile, PRKN expression showed an initial increase at 6 h (2.57-fold), followed by a decrease at 12 h (0.73-fold), and a further slight increase at 24 h (0.99-fold). In the presence of CL LUVs, PINK1 exhibited a relative expression of 4.54 at 6 h, followed by 0.88 at 12 h and 0.99 at 24 h. Similarly, PRKN displayed a relative expression of 2.52 at 6 h, 0.78 at 12 h, and 0.71 at 24 h.

Furthermore, our analysis encompassed the gene expression of proteins associated with the mt-UPS pathways in samples treated with $A\beta_{1-42}$ formed in the presence of PC:Cho LUVs. Notably, PINK1 relative expression was remarkably low at 6 h (0.02-fold), followed by an increase to 0.48-fold at 12 h and a further increase to 1.46-fold at 24 h. Conversely, PRKN relative expression was 0.43-fold at 6 h, followed by 0.71-fold at 12 h, and 1.18-fold at 24 h.

2.4. *External rather than internal damage of MT caused by $A\beta_{1-42}$ fibrils that were grown with and without LUVs*

We used the JC-1 assay combined with flow cytometry and fluorescence microscopy to investigate the dynamics of MT impairment caused by $A\beta_{1-42}$ fibrils were grown with and without LUVs at 6, 12, and 24 h after the exposition of N27 cells to amyloid aggregates.

After 6 h, the magnitude of the JC-1 signal was significantly higher in all fibril-treated groups compared to the control group, Fig. 3(a). Specifically, $A\beta_{1-42}$:PC showed the highest JC-1 response (60.5 % ± 2 %), followed by $A\beta_{1-42}$:PC:Cho (51.5 % ± 2 %), $A\beta_{1-42}$ (37.2 % ± 2 %), and $A\beta_{1-42}$:CL (34.4 % ± 4 %). We observed a progressive increase in JC-1 intensities in all groups as the time of the cell exposition to protein aggregates increased. Specifically, JC-1 intensity increased for $A\beta_{1-42}$ from 46.5 % ± 4 % (12*h*) to 51.7 % ± 8.4 % (24 h), whereas for $A\beta_{1-42}$:PC, we observed an increase from 86.4 % ± 4 % (12 h) to 96 % ± 2.8 % (24 h). Similar changes were observed for $A\beta_{1-42}$:CL (49.1 % ± 2 % (12 h) to 70.2 % ± 6.4 % (24 h)) and $A\beta_{1-42}$:PC:Cho (73.6 % ± 3 % (12 h) to 81.8 % ± 8 % (24 h)). Notably, cells grown in the presence of LUVs alone showed a JC-1 signal that was not significantly different from untreated cells, indicating that the observed JC-1 response was due to the presence of fibrils and not to the lipids themselves, Fig. S2(a).

To validate the results obtained from the JC-1 assay using flow cytometry, we performed fluorescence microscopy analysis on N27 cells treated with $A\beta_{1-42}$ fibrils in the presence and absence of PC, CL, and PC:Cho LUVs for 24 h, Fig. 3(c). The images clearly showed a significant increase in green JC-1 fluorescence intensity, indicating a reduction in MT membrane potential, in cells treated with all types of $A\beta_{1-42}$ fibrils as compared to the control cells.

We also used ROS assay to detect and quantify changes in the amounts of ROS in N27 cells after their treatment with amyloid fibrils that were grown with LUVs composed of CL, PC, and PC:Cho, as well as in the absence of lipids. In ROS assay, Deep Red fluorescent dye is used. Live cells are permeable to this dye, which allows for detection and

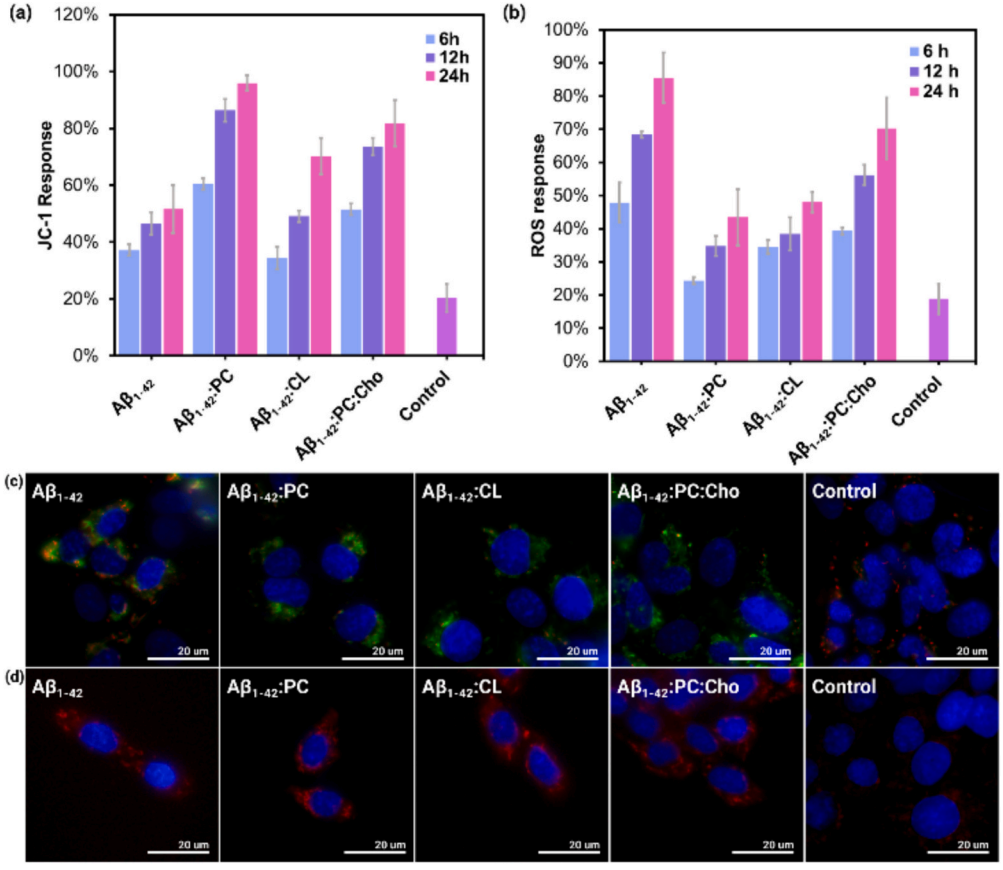

Fig. 3. Histogram of JC-1 a) and ROS b) assays of N27 neuronal cells incubated for 6 h, 12 h, and 24 h with Aβ1–42 fibrils that were grown in LUVs composed of CL, PC, and PC:Cho and with no LUVs (Aβ1–42). Fluorescent images that reveal damaged (green) and healthy (red) mitochondria (c), as well as (d) ROS levels (red) in N27 cells exposed for 24 h to Aβ1–42 fibrils grown in LUVs composed of CL, PC, and PC:Cho and with no LUVs (Aβ1–42); cell nuclei are shown in blue. (For interpretation of the references to colour in this figure legend, the reader is referred to the web version of this article.)

quantification of superoxide and hydroxyl radicals in such cells. In the cytosol, Deep Red is oxidized by ROS producing a derivative that exhibits a strong fluorescence. Consequently, flow cytometry or fluorescence imaging could be used quantify levels of ROS in the cells.

We found that the intensity of the ROS signal increased with time for all samples, with the highest ROS stress observed at 24 h of treatment, Fig. 3(b). The ROS signal from cells after 6 h of incubation with fibrils showed that $A\beta_{1-42}$:PC fibrils had the least cytotoxicity with 24.3 % ± 0.8 % ROS stress, followed by $A\beta_{1-42}$:CL (34.6 % ± 1.6 %) and $A\beta_{1-42}$:PC:Cho (39.3 % ± 0.8 %). ROS stress from $A\beta_{1-42}$ fibrils from a lipid-free environment shows the maximum percentage at the current time point of 47.9 % ± 4.9 %. The ROS signal was significantly higher in all fibril-treated samples compared to the non-treated control (18.9 % ± 3.7 %). We observed a progressive increase in ROS quantities in all groups as the time of the cell exposition to protein aggregates increased. Specifically, ROS intensity increased for $A\beta_{1-42}$ from 68.5 % ± 0.8 % (12 h) to 85.6 % ± 6.2 % (24 h), whereas for $A\beta_{1-42}$:PC we observed an increase from 34.8 % ± 2.4 % (12 h) to 43.5 % ± 6.9 % (24 h). Similar changes were observed for $A\beta_{1-42}$:CL (38.4 % ± 4.1 % (12 h) to 48 % ± 2.5 % (24 h)) and $A\beta_{1-42}$:PC:Cho (56.2 % ± 2.4 % (12 h) to 70.3 % ± 7.5 % (24 h). Notably, cells grown in the presence of LUVs alone showed a ROS signal that was not significantly different from untreated cells, indicating that the observed ROS response was due to the presence of fibrils and not to the lipids themselves, Fig. S2(b).

We also performed fluorescence microscopy on N27 cells treated with $A\beta_{1-42}$ fibrils formed with LUVs composed of CL, PC, and PC:Cho for 24 h, Fig. 3(b). The images clearly showed a significant increase in ROS fluorescence intensity in cells treated with all types of $A\beta_{1-42}$ fibrils as compared to the control cells.

3. Discussion

Amyloid aggregates can directly permeabilize the plasma membrane or get endocytosed by cells. [26,59] In the former case, these toxic species appear in the cytosol where they impair physiological processes necessary to maintain cell homeostasis. [59] In the latter case, amyloid aggregates damage endosomes and leak out into the cytosol. [28] Previously reported results by Matveyenka et al. showed that the endosomal damage was directly linked to enhanced UPR response and severe ER impairment. [28] It was also found that insulin oligomers and fibrils formed in the presence of different phospho- and sphingolipids exerted drastically different endosomal damage and UPR response. [28]

In the current study, we investigated the extent to which morphologically similar $A\beta_{1-42}$ fibrils with drastically different secondary structure caused MT and ER damage. We previously demonstrated that differences in the secondary structure were induced by lipids that were present at the stage of $A\beta_{1-42}$ aggregation. Furthermore, AFM-IR used for analysis of these aggregates revealed the presence of lipids in their structure [23]. Thus, lipids not only altered the secondary structure of these aggregates, but also changed their hydrophobicity. Using qPCR, we observed drastically different patterns of gene expression of ER UPR pathways in cells treated with $A\beta_{1-42}$ fibrils formed in the presence of lipids and a lipid-free environment. When exposed to $A\beta_{1-42}$ fibrils formed in the lipid-free environment, cells showed upregulation of genes involved in the PERK pathway. However, cells treated with $A\beta_{1-42}$:PC exhibited significantly higher upregulation of PERK-related genes and the downregulation of XBP1 and ATF6 genes. $A\beta_{1-42}$:CL and $A\beta_{1-42}$:PC:Cho fibrils caused drastically different changes in the expression of PERK XBP1 and ATF6 genes in N27 cells compared to those observed for $A\beta_{1-42}$ and $A\beta_{1-42}$:PC fibrils. Specifically, these fibrillar species showed a drastic increase of almost PERK genes expression at 6 h with a subsequent downregulation at 12 and 24 h.

Our study revealed a relationship between the relative expression of PERK and ATF4 genes across different treatment conditions and time points. Both PERK and ATF4 exhibited similar trends of up- and down-regulation as a response to amyloid aggregates. This observation suggests that changes in PERK expression can influence the phosphorylation rate of eif2a, subsequently impacting ATF4 expression levels.

The analysis of changes in the expression of genes involved in mt-UPR revealed that $A\beta_{1-42}$:PC:Cho fibrils exhibited the most significant downregulation in gene expression compared to $A\beta_{1-42}$:CL, and $A\beta_{1-42}$:PC, as well as $A\beta_{1-42}$ fibrils. Specifically, the relative expression levels of mt-UPR proteins CLPP, YME1A, UBL-5, PINK, and PRKN were notably suppressed as a result of the cell exposition to $A\beta_{1-42}$ and $A\beta_{1-42}$:PC:Cho fibrils. At the same time, we observed drastically different response of N27 cells to $A\beta_{1-42}$:PC $_{and}$ $A\beta_{1-42}$:CL fibrils. Specifically, we found a strong upregulation of genes responsible for mt-UPR response after the cells were exposed to $A\beta_{1-42}$:PC $_{and}$ $A\beta_{1-42}$:CL fibrils for 6 h with a subsequent downregulation of these genes.

JC-1 assay used in our study indicated progressive MT membrane damage over the course of 24 h after the cell exposition to all protein aggregates. The same results were obtained for the ROS assay that revealed the level of ROS in the cell cytosol. Based on the results of these assays, we can conclude that MT is not directly damaged by amyloid aggregates. Our data suggest that cells facing severe UPR response of ER suppress mt-UPR response enabling the maximal ATP production to mitigate the amyloid-induced stress. Thus, we can conclude that ER damage and increased levels of ROS in the cytosol rather than MT impairment is the primary molecular mechanism by which amyloid aggregates exert their cytotoxicity.

4. Methods

4.1. Large unilamellar vesicles (LUVs) preparation

1,2-Dimyristoyl- glycero-3-phosphocholine (14:0 PC (PC)), Cat. N. 85–0345; 18:00 cardiolipin (CL), Cat. N. 71–0334; and cholesterol (Cho), Cat. N. 700-100 were obtained from Avanti Polar Lipids (Alabaster, AL, USA). To prepare LUVs, PC, and CL were first dissolved in 1× phosphate buffer saline (PBS), pH of 7.4, to 400 μM final concentration. For the 5:95 mol:mol Cho:PC, PC and Cho were first mixed in chloroform. Next, chloroform was evaporated by N_2 gas stream until the lipid film was formed. The resulted film was dissolved in 1xPBS, with a pH of 7.4. To ensure the uniformity and stability of LUVs, all samples were subjected to five cycles in liquid nitrogen and water bath. Finally, lipid solutions subjected to LIPEX® Flow Extruder that had membrane with 100 nm pores (A.M.D. Manufacturing Inc. Cat. N. AM-DPCTE-0100-25C). Formed LUVs were ~ 100 nm in diameter according to Dynamic Light Scattering (DLS), Fig. S1.

4.2. Protein aggregation

Human $A\beta_{1-42}$ used in the experiment (GenScript, Cat. No RP10017) was prepared by dissolving it in 1 ml of 1,1,1, 3,3,3-Hexafluoroisopropanol (HFIP) (Across Organics, code 445–820-500) at a concentration of 1 mg/ml. After a 15 min incubation, HFIP was removed under the N_2 stream, and a protein film was formed. The film was then re-dissolved in 1xPBS, pH 7.4, under continuous vortexing on ice for 25 min. The final concentrations of $A\beta_{1-42}$ and LUVs were 60 μM and 240 μM, respectively. Protein samples were incubated at 25 °C under quiescent conditions for 72 h.

4.3. AFM

5 μL of the sample was drop-casted onto silicon wafers and kept on them for 3 min. After wavers were rinsed by DI water and dried under N_2 gas, AFM imaging was performed on Nano-IR3 system (Bruker, Santa Barbara, CA, USA). Contact-mode AFM tips were used to image samples.

4.4. Dynamic Light Scattering (DLS)

Sizes of LUV vesicles were determined using DynaPro NanoStar DLS

with 90° incident light angle.

4.5. Cell toxicity assays

The N27 rat neurons were cultured in RPMI 1640 Medium (ThermoFisher Scientific); Medium contained 10 % fetal bovine serum (FBS) (Invitrogen, Waltham, MA, USA). On average, each well had 30,000 cells. Cells were kept at 37 °C with 5 % CO_2. After 24 h, the cells fully adhered to the wells. Prior to the experiment, 300 μL of the cell culture medium was taken away; next, 300 μL of RPMI 1640 Medium with 5 % FBS were added. 30 μL of protein samples were added to RPMI 1640 Medium with 5 % FBS prior to mixing with cells. After cell exposition of aggregates for 6 h, 12 h, and 24 h, ROS assay was performed. For this, ROS reagent (C-10422, Invitrogen) was added to N27 cells to the final concentration of 5.0 μM. After that cells were incubated 30 min under the same experimental. Supernatant was removed; cells were washed with 1640 RPMI media including 5 % FBS. Cells were exposed to trypsin and suspended in 200 μL of 1xPBS, pH 7.4. ROS measurements were made using Accuri C6 Flow Cytometer (BD, San Jose, CA, USA). For JC-1 test, which indicates mitochondrial impairment, JC-1 reagent (M-34152 A, Invitrogen) was added to obtain 50 μM of the final concentration; cells were incubated at for 30 min with the reagent. After the supernatant was removed, cells were treated by trypsin and resuspended in 200 μL of the 1xPBS, pH 7.4. Sample measurements were made using the same instrument.

4.6. Fluorescence microscopy imaging

N27 neuron cells were cultured in RPMI 1640 Medium with 10 % FBS in 35 mm dishes with the optical bottom (Cat. N. D3510-1.5N, Cellvis). Approximately 300,000 cells were in one well. After 24 h, RPMI 1640 was replaced with a new RPMI 1640 containing 5 % FBS and protein samples. After 6 h, 12 h, and 24 h after protein aggregates were added, cells were exposed to ROS and JC-1 reagents to the final concentrations of 5 μM and 50 μM, respectively. Next, cells were incubated for 20 min at 37 °C, 5 % CO_2. One drop of NucBlue Live Cell ReadyProbes (Cat. No. R-3760-5, Invitrogen) was added to each sample, and incubated for 5 min. Fluorescence images were taken using EVOS M-5000 Imaging System (Invitrogen), with Olympus UPIanApo 100× oil-objective using and deep red, blue, and green optical filters.

4.7. Gene expression

RNA was extracted from cells following treatment using a GeneJET RNA Purification Kit (Cat. No. K-0732, Thermo Scientific). The concentration and purity of the extracted RNA were determined using a Nano-Drop One Spectrophotometer (ThermoFisher Scientific), ensuring A260/A280 ratios were close to 2.0, indicative of high RNA purity. Complementary DNA (cDNA) was made from 1 μg of total RNA using Super-Script™ 3 Reverse Transcriptase (Cat. No. 1–80,800-93, Invitrogen) with random hexamer primers (Cat. No. 48190011, Invitrogen) in a 20 μL reaction volume.

For quantitative PCR (qPCR), specific primers for each target gene were designed (details provided in Table S1) to ensure specificity and compatibility with qPCR amplification conditions. qPCR reactions were performed on a C1000 Touch Thermal Cycler (Bio-Rad). Each 20 μL reaction mixture contained cDNA template (diluted 1:10), 10 μL of SYBR Green PCR Master Mix (Cat. No. 4309155, Applied Biosystems), gene-specific primers (final concentration 300 nM), and of nuclease-free water. The PCR amplification conditions were as follows: initial denaturation at 95 °C for 10 min, followed by 40 cycles of 95 °C for 15 s (denaturation) and 60 °C for 1 min (annealing/extension). Melting curve analyses were performed at the end of each run to verify the specificity of the PCR products.

Beta-actin was employed as a house-keeping gene for the normalization of expression levels of the target genes. To ensure the reliability of obtained results, non-template controls (NTCs) and positive controls were included in each performed qPCR test.

4.8. Data analysis

Quantification of relative expression of genes of interest was made using Ct method ($2^{-\Delta\Delta Ct}$), where ΔCt is the difference in the threshold cycles between the gene of interest and the house-keeping gene. ΔΔCt represents the difference in ΔCt values between the samples exposed to amyloid aggregates and the control samples. The relative expression levels of genes were calculated and presented as fold changes compared to the control samples.

5. Conclusions

Our results demonstrate that $A\beta_{1-42}$ fibrils formed in the presence of PC, CL, and cholesterol exerted drastically different magnitude and dynamic of mt-UPR and UPR of ER. We found that the opposite dynamics of ER and MT responses in rat dopaminergic cells exposed to $A\beta_{1-42}$:CL fibrils and $A\beta_{1-42}$ aggregates formed in a lipid-free environment. Specifically, $A\beta_{1-42}$ fibrils caused a strong upregulation of both ER UPR and mt-UPR, whereas $A\beta_{1-42}$:CL fibrils, on the other hand, caused do fibrils exhibited greater toxicity regulation of both ER UPR and mt-UPR. We also found that $A\beta_{1-42}$:PC fibrils upregulated ER UPR simultaneously downregulated mt-UPR, whereas $A\beta_{1-42}$:PC:Cho fibrils suppressed the UPR response of ER and upregulated mt-UPR. We also observed progressively increasing ROS production that damages mitochondrial membranes and other cell organelles, ultimately leading to cell death. Correlating the dynamics of gene regulation, we found that ER damage and increased levels of ROS in the cytosol rather than MT impairment was the primary molecular mechanism by which amyloid aggregates exert their cytotoxicity. These findings are consistent with the recently reported analysis of changes in ER UPR and mt-UPR triggered by α-syn fibrils formed in the presence and absence of lipids [38]. Thus, we can conclude that lipid-determined changes in amyloid toxicity is a general phenomenon attributed to protein aggregates formed by different rather than one amyloidogenic protein.

CRediT authorship contribution statement

Kiryl Zhaliazka: Writing – review & editing, Writing – original draft, Visualization, Validation, Methodology, Investigation, Conceptualization. **Dmitry Kurouski:** Writing – review & editing, Writing – original draft, Supervision, Resources, Project administration, Funding acquisition, Conceptualization.

Declaration of competing interest

The authors declare the following financial interests/personal relationships which may be considered as potential competing interests: Dmitry Kurouski reports financial support was provided by Texas A&M University. If there are other authors, they declare that they have no known competing financial interests or personal relationships that could have appeared to influence the work reported in this paper.

Data availability

All data in this study can be provided by the corresponding author if needed.

Acknowledgment

We are grateful to the National Institute of Health for the provided financial support (R35GM142869).

Appendix A. Supplementary data

Supplementary data to this article can be found online at https://doi.org/10.1016/j.bbalip.2024.159510.

References

[1] L. Pieri, K. Madiona, R. Melki, Structural and functional properties of prefibrillar α-synuclein oligomers, Sci. Rep. 6 (2016) 24526.
[2] S.W. Chen, S. Drakulic, E. Deas, M. Ouberai, F.A. Aprile, R. Arranz, S. Ness, C. Roodveldt, T. Guilliams, E.J. De-Genst, D. Klenerman, N.W. Wood, T.P. Knowles, C. Alfonso, G. Rivas, A.Y. Abramov, J.M. Valpuesta, C.M. Dobson, N. Cremades, Structural characterization of toxic oligomers that are kinetically trapped during alpha-synuclein fibril formation, Proc. Natl. Acad. Sci. USA 112 (2015) E1994–E2003.
[3] N. Cremades, S.I. Cohen, E. Deas, A.Y. Abramov, A.Y. Chen, A. Orte, M. Sandal, R. W. Clarke, P. Dunne, F.A. Aprile, C.W. Bertoncini, N.W. Wood, T.P. Knowles, C. M. Dobson, D. Klenerman, Direct observation of the interconversion of normal and toxic forms of alpha-synuclein, Cell 149 (2012) 1048–1059.
[4] M.M. Apetri, N.C. Maiti, M.G. Zagorski, P.R. Carey, V.E. Anderson, Secondary structure of alpha-synuclein oligomers: characterization by raman and atomic force microscopy, J. Mol. Biol. 355 (2006) 63–71.
[5] D. Kurouski, R.P. Van Duyne, I.K. Lednev, Exploring the structure and formation mechanism of amyloid fibrils by Raman spectroscopy: a review, Analyst 140 (2015) 4967–4980.
[6] D.P. Hong, S. Han, A.L. Fink, V.N. Uversky, Characterization of the non-fibrillar alpha-synuclein oligomers, Protein Pept. Lett. 18 (2011) 230–240.
[7] M.G. Iadanza, M.P. Jackson, E.W. Hewitt, N.A. Ranson, S.E. Radford, A new era for understanding amyloid structures and disease, Nat. Rev. Mol. Cell Biol. 19 (2018) 755–773.
[8] M. Joao Saraiva, M. Mendes Sousa, I. Cardoso, R. Fernandes, Familial amyloidotic polyneuropathy: protein aggregation in the peripheral nervous system, J. Mol. Neurosci. 23 (2004) 35–40.
[9] R. Kayed, E. Head, J.L. Thompson, T.M. McIntire, S.C. Milton, C.W. Cotman, C. G. Glabe, Common structure of soluble amyloid oligomers implies common mechanism of pathogenesis, Science 300 (2003) 486–489.
[10] R. Kayed, C.A. Lasagna-Reeves, Molecular mechanisms of amyloid oligomers toxicity, J. Alzheimers Dis. 33 (Suppl. 1) (2013) S67–S78.
[11] T.P. Knowles, M. Vendruscolo, C.M. Dobson, The amyloid state and its association with protein misfolding diseases, Nature reviews 15 (2014) 384–396.
[12] H. Lin, R. Bhatia, R. Lal, Amyloid beta protein forms ion channels: implications for Alzheimer's disease pathophysiology, FASEB J. 15 (2001) 2433–2444.
[13] C.A. McLean, R.A. Cherny, F.W. Fraser, S.J. Fuller, M.J. Smith, K. Beyreuther, A. I. Bush, C.L. Masters, Soluble pool of Abeta amyloid as a determinant of severity of neurodegeneration in Alzheimer's disease, Ann. Neurol. 46 (1999) 860–866.
[14] R. Nelson, D. Eisenberg, Recent atomic models of amyloid fibril structure, Curr. Opin. Struct. Biol. 16 (2006) 260–265.
[15] C.M. Wischik, R.A. Crowther, M. Stewart, M. Roth, Subunit structure of paired helical filaments in Alzheimer's disease, J. Cell Biol. 100 (1985) 1905–1912.
[16] C.M. Wischik, M. Novak, H.C. Thogersen, P.C. Edwards, M.J. Runswick, R. Jakes, J. E. Walker, C. Milstein, M. Roth, A. Klug, Isolation of a fragment of tau derived from the core of the paired helical filament of Alzheimer disease, Proc. Natl. Acad. Sci. USA 85 (1988) 4506–4510.
[17] F. Chiti, C.M. Dobson, Protein misfolding, amyloid formation, and human disease: a summary of progress over the last decade, Annu. Rev. Biochem. 86 (2017) 27–68.
[18] M. Serra-Batiste, M. Ninot-Pedrosa, M. Bayoumi, M. Gairi, G. Maglia, N. Carulla, Abeta42 assembles into specific beta-barrel pore-forming oligomers in membrane-mimicking environments, Proc. Natl. Acad. Sci. USA 113 (2016) 10866–10871.
[19] M. Eto, T. Hashimoto, T. Shimizu, T. Iwatsubo, Characterization of the unique in vitro effects of unsaturated fatty acids on the formation of amyloid β fibrils, PLoS One 14 (2019) e0219465.
[20] P. Khatua, A.K. Jana, U.H.E. Hansmann, Effect of lauric acid on the stability of Aβ42 oligomers, ACS Omega, 6 5795–5804.
[21] R. Cataldi, S. Chia, K. Pisani, F.S. Ruggeri, C.K. Xu, T. Sneideris, M. Perni, S. Sarwat, P. Joshi, J.R. Kumita, S. Linse, J. Habchi, T.P.J. Knowles, B. Mannini, C. M. Dobson, M. Vendruscolo, A dopamine metabolite stabilizes neurotoxic amyloid-beta oligomers, Commun Biol 4 (2021) 19.
[22] A.S. Johansson, A. Garlind, F. Berglind-Dehlin, G. Karlsson, K. Edwards, P. Gellerfors, F. Ekholm-Pettersson, J. Palmblad, L. Lannfelt, Docosahexaenoic acid stabilizes soluble amyloid-β protofibrils and sustains amyloid-β-induced neurotoxicity in vitro, FEBS J. 274 (2007) 990–1000.
[23] K. Zhaliazka, M. Matveyenka, D. Kurouski, Lipids uniquely Alter the secondary structure and toxicity of amyloid beta 1-42 aggregates, FEBS J. 290 (2023) 3203–3220.
[24] M. Matveyenka, S. Rizevsky, D. Kurouski, Unsaturation in the fatty acids of phospholipids drastically alters the structure and toxicity of insulin aggregates grown in their presence, J. Phys. Chem. Lett. (2022) 4563–4569.
[25] M. Matveyenka, S. Rizevsky, D. Kurouski, Length and unsaturation of fatty acids of phosphatidic acid determines the aggregation rate of insulin and modifies the structure and toxicity of insulin aggregates, ACS Chem. Neurosci. 13 (2022) 2483–2489.
[26] M. Matveyenka, S. Rizevsky, D. Kurouski, Amyloid aggregates exert cell toxicity causing irreversible damages in the endoplasmic reticulum, Biochim. Biophys. Acta Mol. basis Dis. 1868 (2022) 166485.
[27] M. Matveyenka, S. Rizevsky, D. Kurouski, The degree of unsaturation of fatty acids in phosphatidylserine alters the rate of insulin aggregation and the structure and toxicity of amyloid aggregates, FEBS Lett. 596 (2022) 1424–1433.
[28] M. Matveyenka, S. Rizevsky, J.P. Pellois, D. Kurouski, Lipids uniquely alter rates of insulin aggregation and lower toxicity of amyloid aggregates, Biochim. Biophys. Acta Mol. Cell Biol. Lipids 1868 (2023) 159247.
[29] M. Matveyenka, K. Zhaliazka, S. Rizevsky, D. Kurouski, Lipids uniquely alter secondary structure and toxicity of lysozyme aggregates, FASEB J. 36 (2022) e22543.
[30] M.F. Sciacca, F. Lolicato, G. Di Mauro, D. Milardi, L. D'Urso, C. Satriano, A. Ramamoorthy, C. La Rosa, The role of cholesterol in driving IAPP-membrane interactions, Biophys. J. 111 (2016) 140–151.
[31] M.F.M. Sciacca, R. Chillemi, S. Sciuto, V. Greco, C. Messineo, S.A. Kotler, D.K. Lee, J.R. Brender, A. Ramamoorthy, C. La Rosa, D. Milardi, A blend of two resveratrol derivatives abolishes hIAPP amyloid growth and membrane damage, Biochim. Biophys. Acta Biomembr. 2018 (1860) 1793–1802.
[32] N.P. Alza, P.A. Iglesias Gonzalez, M.A. Conde, R.M. Uranga, G.A. Salvador, Lipids at the crossroad of alpha-synuclein function and dysfunction: biological and pathological implications, Front. Cell. Neurosci. 13 (2019) 175.
[33] B.K. Choi, M.G. Choi, J.Y. Kim, Y. Yang, Y. Lai, D.H. Kweon, N.K. Lee, Y.K. Shin, Large alpha-synuclein oligomers inhibit neuronal SNARE-mediated vesicle docking, Proc. Natl. Acad. Sci. USA 110 (2013) 4087–4092.
[34] A. Iyer, N. Schilderink, M. Claessens, V. Subramaniam, Membrane-bound alpha synuclein clusters induce impaired lipid diffusion and increased lipid packing, Biophys. J. 111 (2016) 2440–2449.
[35] L. Kjaer, L. Giehm, T. Heimburg, D. Otzen, The influence of vesicle size and composition on alpha-synuclein structure and stability, Biophys. J. 96 (2009) 2857–2870.
[36] J. Sitton, A. Ali, L. Osborne, A.P. Holman, A. Rodriguez, D. Kurouski, Plasmalogens alter the aggregation rate of transthyretin and lower toxicity of transthyretin fibrils, J. Phys. Chem. Lett. 15 (2024) 4761–4766.
[37] I. Farid, A. Ali, A.P. Holman, L. Osborne, D. Kurouski, Length and saturation of choline plasmalogens alter the aggregation rate of alpha-synuclein but not the toxicity of amyloid fibrils, Int. J. Biol. Macromol. 264 (2024) 130632.
[38] K. Zhaliazka, A. Ali, D. Kurouski, Phospholipids and cholesterol determine molecular mechanisms of cytotoxicity of alpha-synuclein oligomers and fibrils, ACS Chem. Neurosci. 15 (2024) 371–381.
[39] C. Tempra, F. Scollo, M. Pannuzzo, F. Lolicato, C. La Rosa, A unifying framework for amyloid-mediated membrane damage: the lipid-chaperone hypothesis, Biochim. Biophys. Acta, Proteins Proteomics 1870 (2022) 140767.
[40] C. La Rosa, S. Scalisi, F. Lolicato, M. Pannuzzo, A. Raudino, Lipid-assisted protein transport: a diffusion-reaction model supported by kinetic experiments and molecular dynamics simulations, J. Chem. Phys. 144 (2016) 184901.
[41] K.J. Korshavn, C. Satriano, Y. Lin, R. Zhang, M. Dulchavsky, A. Bhunia, M. I. Ivanova, Y.H. Lee, C. La Rosa, M.H. Lim, A. Ramamoorthy, Reduced lipid bilayer thickness regulates the aggregation and cytotoxicity of amyloid-beta, J. Biol. Chem. 292 (2017) 4638–4650.
[42] F. Scollo, C. Tempra, F. Lolicato, M.F.M. Sciacca, A. Raudino, D. Milardi, C. La Rosa, Phospholipids critical micellar concentrations trigger different mechanisms of intrinsically disordered proteins interaction with model membranes, J. Phys. Chem. Lett. 9 (2018) 5125–5129.
[43] M.F. Sciacca, F. Lolicato, C. Tempra, F. Scollo, B.R. Sahoo, M.D. Watson, S. Garcia-Vinuales, D. Milardi, A. Raudino, J.C. Lee, A. Ramamoorthy, C. La Rosa, Lipid-chaperone hypothesis: a common molecular mechanism of membrane disruption by intrinsically disordered proteins, ACS Chem. Neurosci. 11 (2020) 4336–4350.
[44] F. Urano, A. Bertolotti, D. Ron, IRE1 and efferent signaling from the endoplasmic reticulum, J. Cell Sci. 113 (Pt 21) (2000) 3697–3702.
[45] M. Calfon, H. Zeng, F. Urano, J.H. Till, S.R. Hubbard, H.P. Harding, S.G. Clark, D. Ron, IRE1 couples endoplasmic reticulum load to secretory capacity by processing the XBP-1 mRNA, Nature 415 (2002) 92–96.
[46] X. Shen, R.E. Ellis, K. Lee, C.Y. Liu, K. Yang, A. Solomon, H. Yoshida, R. Morimoto, D.M. Kurnit, K. Mori, R.J. Kaufman, Complementary signaling pathways regulate the unfolded protein response and are required for *C. elegans* development, Cell 107 (2001) 893–903.
[47] C.J. Adams, M.C. Kopp, N. Larburu, P.R. Nowak, M.M.U. Ali, Structure and molecular mechanism of ER stress signaling by the unfolded protein response signal activator IRE1, Front. Mol. Biosci. 6 (2019) 11.
[48] M.C. Kopp, N. Larburu, V. Durairaj, C.J. Adams, M.M.U. Ali, UPR proteins IRE1 and PERK switch BiP from chaperone to ER stress sensor, Nat. Struct. Mol. Biol. 26 (2019) 1053–1062.
[49] A.H. Lee, N.N. Iwakoshi, L.H. Glimcher, XBP-1 regulates a subset of endoplasmic reticulum resident chaperone genes in the unfolded protein response, Mol. Cell. Biol. 23 (2003) 7448–7459.
[50] N.N. Iwakoshi, A.H. Lee, L.H. Glimcher, The X-box binding protein-1 transcription factor is required for plasma cell differentiation and the unfolded protein response, Immunol. Rev. 194 (2003) 29–38.
[51] A.H. Lee, N.N. Iwakoshi, K.C. Anderson, L.H. Glimcher, Proteasome inhibitors disrupt the unfolded protein response in myeloma cells, Proc. Natl. Acad. Sci. USA 100 (2003) 9946–9951.
[52] H.P. Harding, Y. Zhang, D. Ron, Protein translation and folding are coupled by an endoplasmic-reticulum-resident kinase, Nature 397 (1999) 271–274.
[53] J. Sok, X.Z. Wang, N. Batchvarova, M. Kuroda, H. Harding, D. Ron, CHOP-dependent stress-inducible expression of a novel form of carbonic anhydrase VI, Mol. Cell. Biol. 19 (1999) 495–504.

[54] F. Urano, X. Wang, A. Bertolotti, Y. Zhang, P. Chung, H.P. Harding, D. Ron, Coupling of stress in the ER to activation of JNK protein kinases by transmembrane protein kinase IRE1, Science 287 (2000) 664–666.
[55] N. Al-Furoukh, A. Ianni, H. Nolte, S. Holper, M. Kruger, S. Wanrooij, T. Braun, ClpX stimulates the mitochondrial unfolded protein response (UPRmt) in mammalian cells, Biochim. Biophys. Acta 2015 (1853) 2580–2591.
[56] B. Schreiner, H. Westerburg, I. Forne, A. Imhof, W. Neupert, D. Mokranjac, Role of the AAA protease Yme1 in folding of proteins in the intermembrane space of mitochondria, Mol. Biol. Cell 23 (2012) 4335–4346.
[57] S.A. Broadley, F.U. Hartl, Mitochondrial stress signaling: a pathway unfolds, Trends Cell Biol. 18 (2008) 1–4.
[58] R.J. Youle, D.P. Narendra, Mechanisms of mitophagy, Nat. Rev. Mol. Cell Biol. 12 (2011) 9–14.
[59] S. Srinivasan, S. Patke, Y. Wang, Z. Ye, J. Litt, S.K. Srivastava, M.M. Lopez, D. Kurouski, I.K. Lednev, R.S. Kane, W. Colon, Pathogenic serum amyloid A 1.1 shows a long oligomer-rich fibrillation lag phase contrary to the highly amyloidogenic non-pathogenic SAA2.2, J. Biol. Chem. 288 (2013) 2744–2755.